Journal of Energy Storage 180 (2026) 124255

Contents lists available at ScienceDirect

Journal of Energy Storage

journal homepage: www.elsevier.com/locate/est

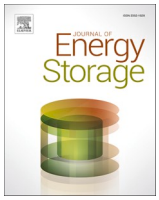

Research papers

Cation-aromatic nitrogen interaction as a design principle for sodium deep eutectic electrolytes

Eudes Eterno Fileti [a,*], Luis G. Dias [b], G. Camilo [c], Dinis O. Abranches [c], João A.P. Coutinho [c]

[a] Instituto de Ciência e Tecnologia, Universidade Federal de São Paulo, 12247-014, São José dos Campos, SP, Brazil
[b] Chemistry Department, FFCLRP, University of São Paulo, 14040-901, Ribeirão Preto, SP, Brazil
[c] CICECO – Aveiro Institute of Materials, Department of Chemistry, University of Aveiro, Aveiro, 3810-193, Portugal

ARTICLE INFO

Keywords:
Sodium-ion batteries
Deep eutectic electrolytes
NaFSI
Imidazole
Aromaticity
Ionic conductivity
Molecular dynamics

ABSTRACT

We report a combined experimental and ab initio molecular dynamics investigation into the role of nitrogen hybridization (sp^2 vs sp^3) and ring aromaticity in the sodium-based deep eutectic electrolyte formation and their potential use in sodium-ion battery electrolytes. Mixtures of NaFSI with three amines at 1:4 M ratio reveal a sharp dependence on amine electronic structure: aromatic 1,2-dimethylimidazole (DMIm) and 1-methylimidazole (MIm) readily dissolve NaFSI, whereas non-aromatic *N*-methylpyrrolidine (MPy) leads to phase separation. AIMD simulations of NaFSI/DMIm, NaFSI/Im, and NaFSI/MPy demonstrate that in aromatic systems Na^+ forms directional coordination with the sp^2 lone pair of the imidazole –N=C– nitrogen, while in MPy the sp^3 nitrogen fails to stabilize Na^+, leaving it ion-paired with FSI^- and driving salt clustering. Composition-dependent AIMD of NaFSI/DMIm (1:1, 1:4, 1:8) shows a monotonic exchange of Na…O for Na…N contacts as DMIm content increases, with coordination numbers confirming a genuine enthalpic preference for imidazole nitrogen over FSI oxygen. The NaFSI/DMIm (1:4) electrolyte exhibits moderate viscosity (49.3 ± 3.7 cP) and ionic conductivity (1.24 ± 0.02 mS cm^{-1}), with Walden plot analysis showing a higher ionicity than for most conventional DES. These results identify the sp^2 hybridization of the coordinating nitrogen as a key design principle for deep eutectic electrolyte formation, supported here by a controlled three-system comparison that isolates the roles of aromaticity and nitrogen hybridization, and providing a basis for the rational design of safer and more efficient sodium-ion battery electrolytes.

1. Introduction

Rechargeable sodium-ion batteries (SIBs) are attractive alternatives to lithium systems because of sodium's abundance and similar redox chemistry. [1,2] However, since carbonate electrolytes are flammable and pose safety risks, low or non-volatile media such as ionic liquids and deep eutectic solvents (DESs) have therefore emerged as promising, safer alternatives. [3] DESs are a subclass of eutectic solvents formed by mixtures of Lewis or Brønsted acids and bases whose strong, favorable interactions induce enthalpy-driven negative deviations from ideality, leading to unusually deep melting point depressions. [4] These systems combine low vapor pressure and tunability of viscosity/ionicity, and recent reports show that they can be tailored to solvate Na^+ efficiently in battery contexts. [5,6]

Deep eutectic electrolytes (DEEs) are a class of advanced and sustainable electrolytes derived from DESs, specifically designed for applications in energy storage devices, such as batteries and supercapacitors. Recent studies on DEEs have shown promising performance in SIB half-cells. [6,7] Xiong et al. [6] introduced a novel DEE by dissolving NaFSI salt in 1,2-dimethylimidazole (DMIm), showing that the strong Na…N coordination could produce a liquid with low viscosity, high ionic conductivity and a 3.2 V stability window. Spectroscopy (Raman, ^{23}Na NMR) confirmed that the imidazole N atom binds Na^+ (a Lewis acid) and thereby liberates Na^+ from the salt. This DEE exhibited high Na^+ conductivity and reversible capacity with excellent cycling stability. [6,8,9] By contrast, conventional IL electrolytes are often difficult to design and viscous, which limits conductivity and capacity. For instance, Monti et al. [5] showed that imidazolium-TFSI ionic liquids require careful design to solvate Na^+ effectively (often yielding moderate conductivities and low Na^+ transference). Overall, DES-based electrolytes promise safer operation with tunable properties, but their investigation in SIBs remains in its infancy. Only a few systems (e.g.

* Corresponding author.
E-mail addresses: fileti@unifesp.br (E.E. Fileti), lgdias@ffclrp.usp.br (L.G. Dias), jdinis@ua.pt (D.O. Abranches), jcoutinho@ua.pt (J.A.P. Coutinho).

https://doi.org/10.1016/j.est.2026.124255
Received 28 April 2026; Received in revised form 24 July 2026; Accepted 16 August 2026
Available online 22 August 2026

NaFSI/DMIm or NaFSI/NMA) have been reported, and the mechanisms by which Na^+ is coordinated and transported remain underexplored and poorly understood. [6,8,9]

The Na…N interaction in the NaFSI/DMIm DEE is rather unusual and appears to be essential. The imidazole ring contains a Lewis-basic nitrogen (the pyridine-like N) that can coordinate Na^+, forming a transient Na…N bond. This ion-dipole coordination is weaker than a covalent bond but strong enough to dissociate the salt and create mobile Na^+ carriers. [6,9] By contrast, a saturated cyclic amine such as *N*,*N*-dimethylpyrrolidine (MPy), without an aromatic π-system, has a different electronic structure and basicity, so its Na…N coordination should differ. Studies in ionic liquid media have shown that aromatic imidazolium vs aliphatic pyrrolidinium environments can markedly change amine basicity and ion-pair stability. [10] This contrast reveals a distinct mechanism. Unlike conventional DES, sodium-based DEEs are stabilized by coordination rather than hydrogen bonding. In these systems, Na^+ seems to act as a Lewis acid interacting with electron-rich nitrogen sites, giving rise to a coordination-driven eutectic environment rather than a hydrogen-bonded one. This mechanism suggests that the sodium ion plays an active structural role within the electrolyte, beyond its function as a mobile charge carrier. The effectiveness of this interaction is expected to depend critically on the electronic nature of the coordinating molecule. Aromatic nitrogen-containing compounds, such as imidazole derivatives, offer delocalized electronic environments that may stabilize Na···N coordination, whereas non-aromatic amines may not support comparable interactions. Disentangling these effects requires a molecular-level description capable of capturing both electronic structure and thermal fluctuations. Understanding the Na…N bonding environment is important because it directly affects viscosity, conductivity, and electrochemical stability. For instance, altered Na^+ coordination environments have been linked to significantly different ion transport, [11] hence, we expect that the dynamic Na…N interactions will be a key factor in controlling the electrolyte behavior in our systems.

Ab initio molecular dynamics (AIMD) [12] provides a suitable framework to address these challenges, as it enables direct observation of the dynamic coordination of Na^+ in the liquid phase while accounting for electronic polarization and charge transfer effects. Unlike classical force-field MD, AIMD can capture polarization, charge transfer, and the breaking/forming of coordination bonds on the fly. Prior computational work has shown how Na^+ is stabilized by a dense network of non-covalent interactions in eutectic mixtures. [13]

In this work, AIMD is employed to elucidate the role of aromaticity in stabilizing Na···N interactions across different compositions, offering fundamental insight into the design of deep eutectic electrolytes for sodium-ion batteries. We therefore compare the aromatic imidazole-based systems (DMIm and Im) with a non-aromatic analog (MPy) to isolate the role of aromaticity and substitution. By examining these various compounds we aim to isolate how ring aromaticity and geometry affect Na^+ solvation and DEE formation. AIMD will track the time-resolved Na…N coordination, solvation shell, and any transient binding to the anion or solvent. Such simulations provide mechanistic insight (e.g. showing which N sites bind Na^+ and how often) that is difficult to obtain experimentally or via classical models. This molecular-level picture is critical for understanding DEE formation, why its conductivity is high, and how aromaticity alters the coordination dynamics, providing guidelines for the Na-based DEE design.

2. Methodology

2.1. Preparation of deep eutectic electrolytes

N-methylpyrrolidine (Mpy, >98%, Alfa Aesar), 1-methylimidazole (Mim, >99%, Acros Organics), 1,2-dimethylimidazole (DMIm, >98%, Sigma-Aldrich), and sodium bis(fluorosulfonyl)imide (NaFSI, >95%, Fluorochem) were used as received without further purification. Deep eutectic electrolyte systems based on NaFSI/Mpy, NaFSI/Mim, and NaFSI/DMIm were prepared at molar ratios of 1:4 (NaFSI:base) by weighing gravimetrically ($\pm 10^{-4}$ g) the DEE components in sealed glass vials, and magnetically stirred at 333 K for 1 h to ensure complete homogenization. The mixtures were then allowed to cool naturally to ambient temperature and left undisturbed for at least 5 h. The macroscopic appearance of the samples was visually monitored after cooling to assess miscibility and phase homogeneity. These experimental observations were used for comparison with computational predictions of mixing behavior and structural organization. [6]

2.2. Characterization of the DEEs

The NaFSI/DMIm (1:4) system was characterized in terms of viscosity and ionic conductivity. Viscosity measurements were performed at four different temperatures (298, 308, 318, and 328 K) using a cone-plate rotational viscometer (RM 100 CP-2000 PLUS, Lamy Rheology). [14] Temperature control was maintained using the instrument's integrated thermal regulation system, and measurements were conducted after thermal equilibration at each set temperature. Ionic conductivity was measured at 298 K using a SevenExcellence S470 conductivity meter (Mettler-Toledo) equipped with a calibrated conductivity probe. [15] Prior to measurements, the instrument was calibrated using standard conductivity solutions according to the manufacturer's recommendations. All measurements were performed in triplicate to ensure reproducibility and reliability of the results. The reported viscosity values correspond to the mean of three independent measurements, with the standard deviation provided as the uncertainty estimate. The main sources of experimental error include the specified accuracy of the cone-plate geometry (± 2.5% of reading, as stated by the manufacturer), temperature fluctuations within the regulation tolerance of ±0.1 K, and variability across replicate sample loadings.

2.3. Classical molecular dynamics and pre-equilibration

Initial configurations for the atomistic simulations were generated using the Packmol software [16] ensuring homogeneous distributions of ring systems (DMIm, MPy and Im) and NaFSI ion pairs within cubic simulation cells. Separate simulations were also performed for the isolated components (a single ring system and an isolated NaFSI ion pair) to establish reference structural and energetic benchmarks. Three deep eutectic systems at a molar ratio of 1:4 (NaFSI:base) were considered: NaFSI/DMIm, NaFSI/Im and NaFSI/MPy. For the former, 1:1 and 1:8 M ratio were also investigated. The unsubstituted imidazole (Im) system was included as a minimal aromatic reference, allowing the specific Na^+-ring interaction to be isolated from the steric and electronic effects introduced by the *N*-methyl substituents present in DMIm.

Classical molecular dynamics (CMD) simulations were employed as a pre-equilibration step to obtain well-relaxed liquid configurations prior to ab initio molecular dynamics. The OPLS-AA force field [17] was used to describe intra- and intermolecular interactions. Each system was equilibrated in the NPT ensemble at 300 K and 1 bar for 10 ns using the GROMACS 2024 package. [18] The systems exhibited markedly different structural behaviors during pre-equilibration. The NaFSI/DMIm and NaFSI/Im systems evolved into a homogeneous liquid phase, whereas the NaFSI/MPy system showed a strong tendency toward phase segregation, with the formation of a single aggregated salt-rich domain. The configurations from CMD were subsequently used as starting points for AIMD simulations in order to investigate the role of molecular structure, particularly aromaticity, in governing ion coordination and mixing behavior of the NaFSI/DMIm solution. These CMD simulations were not used for structural analysis but solely to provide physically reasonable starting geometries for AIMD, minimizing spurious artifacts related to initial packing.

2.4. Ab initio molecular dynamics simulations

The final configurations obtained from CMD were used as starting points for ab initio molecular dynamics simulations. Electronic structure calculations were performed within density functional theory (DFT) using the BLYP functional augmented with Grimme's D3 dispersion correction (BLYP-D3). [19–21] This functional was chosen due to its proven reliability in describing non-covalent interactions, ion-dipole coordination, and vibrational properties in ionic liquids and eutectic systems. [22–25] Core electrons were treated using Goedecker-Teter-Hutter (GTH) pseudopotentials, [26] and the valence electronic structure was expanded in a double-ζ MOLOPT-DZVP-SR-GTH basis set. [27] Plane-wave and relative cutoffs were set to 350 Ry and 40 Ry, respectively, and the self-consistent field (SCF) convergence criterion was fixed at 10^{-6}. All AIMD simulations were performed in the NVT ensemble at 300 K using the QUICKSTEP module [27] of the CP2K software package. [28] Each system was equilibrated for 5 ps, followed by a 30 ps production run. System compositions, cell dimensions, and simulation times are summarized in Table 1, while representative molecular configurations are shown in Fig. 1. Structural and dynamical analyses were conducted using the TRAVIS program [29] and GROMACS analysis tools. [18] Particular emphasis was placed on characterizing the Na···N coordination through radial distribution functions, coordination number analyses, and time-resolved Na…N distance trajectories. Vibrational power spectra were also computed from the AIMD trajectories and compared qualitatively with the experimental Raman data to establish structure-spectroscopy correlations.

3. Results and discussion

The aromatic character of the imidazole ring has been claimed to play a pivotal role in the stabilization of the deep eutectic electrolytes studied here. By Hückel's rule the imidazole ring is aromatic (6 π electrons, planar), and only one nitrogen (the –N=C– site) retains a pyridine-like lone pair available for Lewis-base coordination to Na^+; the other nitrogen (–N–CH_3) is involved in the π system and is less accessible. Consequently, Na^+ coordination is expected to occur preferentially at the –N=C– site, whose sp^2 lone pair provides a directional Lewis-base interaction with the cation. To isolate the role of nitrogen hybridization and aromaticity we compare DMIm (aromatic, sp^2 nitrogen) with a non-aromatic tertiary amine (MPy, sp^3 nitrogen), which provides a contrasting coordination environment for Na^+.

Visual inspection of the prepared NaFSI-amine mixtures (Fig. 2) revealed a striking dependence on amine structure. The NaFSI+MPy (1:4) sample showed clear phase separation: a dense yellow salt-rich layer settled at the bottom with a clear upper phase (indicating the non-solubilization of NaFSI). In contrast, the NaFSI+MIm mixture was nearly homogeneous, exhibiting only slight turbidity (minor scattering) but no macroscopic layering. Remarkably, the NaFSI+DMIm sample remained fully homogeneous and optically transparent, with no visible precipitate. These observations indicate that the aromatic imidazole derivatives (MIm, DMIm) solvate the Na salt far better than the non-aromatic pyrrolidine (MPy), which leads to salt exclusion and aggregation.

Table 1
Typical specifications of the simulated deep eutectic electrolytes (DEE-1:X) and its components, including the number of ion pairs and DMIm molecules, total atom count and dimension of the computational cell (in pm). Total simulation time (equilibration and production, in ps).

System	# IP	# DMIn	# Atoms	Box size (pm)	Time
Isolated DMIm	0	1	15	1800	1 + 10 ps
Isolated Na/FSI pair	1	0	10	1800	1 + 10 ps
DEE-1:8 (DMIm)	4	32	520	1753	5 + 30 ps
DEE-1:4 (DMIm)	8	32	560	1820	5 + 30 ps
DEE-1:1 (DMIm)	20	20	500	1946	5 + 30 ps
DEE-1:4 (Im)	9	36	414	1732	5 + 30 ps
DEE-1:4 (MPy)	7	28	630	1826	5 + 30 ps

The NaFSI/MPy system developed strong ion clustering: Na^+ ions and FSI^- anions aggregated into dense domains, consistent with a salt-rich precipitate (as observed experimentally). Similar behavior was seen in AIMD and CMD simulations of the NaFSI/MPy mixture (non-aromatic tertiary amine): NaFSI was largely excluded from the bulk liquid, forming separate salt clusters under all equilibration protocols. By contrast, AIMD and CMD of the NaFSI/DMIm system showed complete miscibility. In these simulations every Na^+ remained well dispersed and strongly coordinated by DMIm molecules, with no persistent NaFSI clusters. Thus, the simulations reproduce the experimental trend: MPy, and other non-aromatic amines, such as Triethylamine (TEA) [30] and *N*-methylacetamide (NMA), [7] fail to keep NaFSI in solution, whereas the aromatic DMIm binds Na^+ tightly, preventing salt-liquid phase separation. Notably, prior spectroscopic studies similarly noted extensive Na^+-FSI^- aggregation in high-salt concentration mixtures lacking strong ligands able to donate electron density to Na. [31] Our MD results echo this result, showing the same salt-rich aggregates when Na^+ is not effectively stabilized by the solvent.

Mechanistically, these results can be understood from the electronic structure of the amines. In non-aromatic MPy and DMPy, the nitrogen's lone pair resides in an sp^3-like orbital and there is no conjugated π-system for additional stabilization; thus Na^+ has limited coordination sites and remains largely bound to FSI^-, leading to salt clustering. In contrast, DMIm contains an imidazole ring with one nitrogen (–N=C–) that has an accessible sp^2 lone pair and an extended π-system. This aromatic N=C unit acts as a Lewis base toward Na^+, providing a directional coordination site that is absent in non-aromatic amines. The accessible sp^2 lone pair of DMIm therefore provides an effective binding site for Na^+, allowing salt solubilization. This picture is consistent with prior observations of Na^+ coordination in similar systems. [32]

To assess the role of aromaticity in governing Na^+ coordination, RDFs and CNs were computed from AIMD simulations of the three 1:4 NaFSI/base systems (NaFSI/DMIm, NaFSI/Im, and NaFSI/MPy) and are presented comparatively in Fig. 3. It should be noted that the NaFSI/MPy system is phase-separated under these conditions (cf. Fig. 2a), so that the Na-centred RDFs computed for MPy describe the local structure within the salt-rich precipitate rather than a homogeneous liquid; MPy is included here as a negative structural control to diagnose the coordination failure that underlies the experimentally observed phase separation. This three-system comparison was designed to isolate a single structural variable (the hybridization state and aromatic character of the coordinating nitrogen) while keeping the salt, stoichiometry, and simulation protocol identical, so that any difference in Na^+ coordination can be attributed directly to the electronic structure of the amine. The top row shows the Na…N RDF and its running integral (CN), while the bottom row presents the corresponding Na…O interactions. The Na…N RDF reveals a well-defined first coordination peak at approximately 240 pm for both aromatic systems (DMIm and Im), consistent with a direct Na^+-nitrogen interaction at the imidazole –N=C– site. The peak is most intense for DMIm, followed by Im, indicating a slightly stronger Na···N coordination in DMIm. This difference likely arises from subtle electronic and structural effects associated with methyl substitution, although the dominant factor remains the presence of an aromatic sp^2 nitrogen site. In contrast, the MPy system displays a considerably weaker Na…N signal, with a lower and broader first peak, reflecting the poor ability of the non-aromatic sp^3 nitrogen to coordinate Na^+ in a directed fashion. The corresponding CN curves corroborate this trend: the Na…N coordination number at the first shell minimum is highest for DMIm, intermediate for Im, and substantially reduced for MPy.

The Na…O RDF, however, tells the opposite story. The MPy system exhibits a strikingly intense first peak at ~240 pm, the highest among the three systems by a large margin, indicating that Na^+ is almost exclusively coordinated by FSI^- oxygens in the absence of effective amine solvation. This is fully consistent with the macroscopic phase

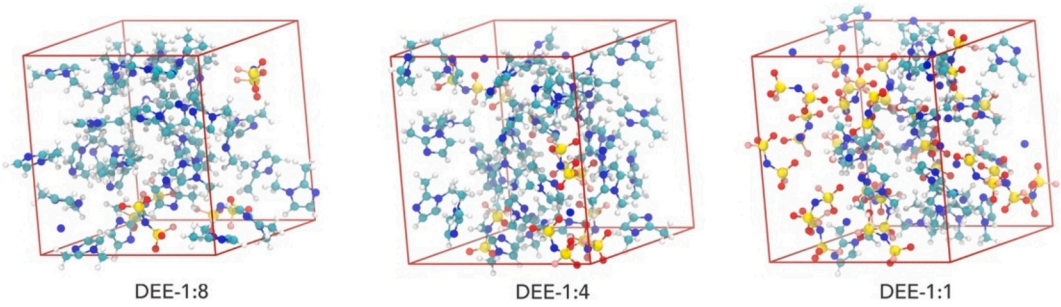

Fig. 1. Molecular configurations of the DEEs studied. From left to right the box with pure DMIm, and the three mixtures, in different molar ratio of DMIm/NaFSI, 1:8, 1:4 and 1:1.

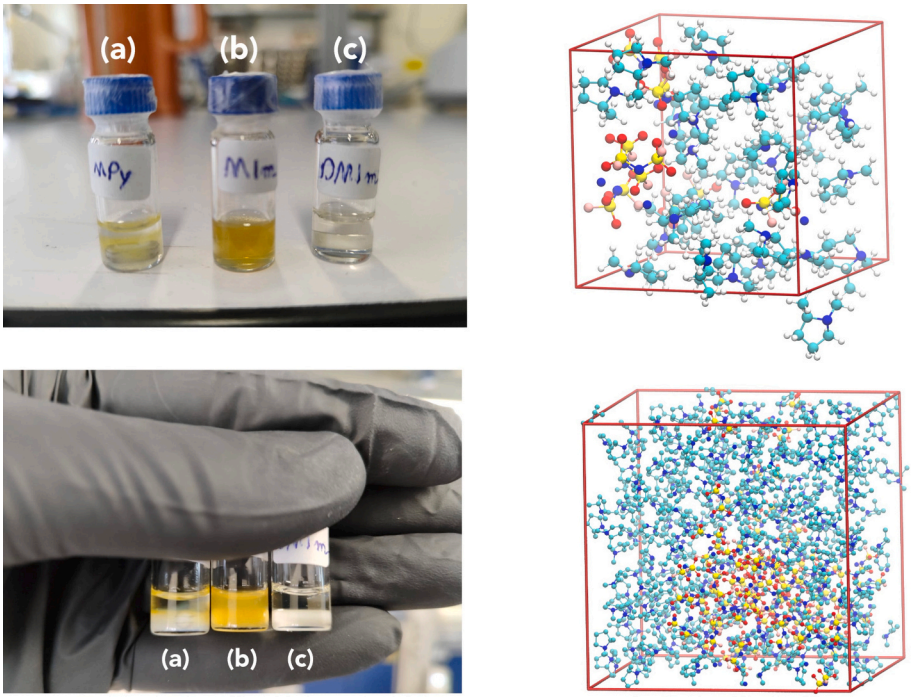

Fig. 2. At left, the visual aspect of NaFSI (1:4 NaFSI:amine) mixtures after equilibration: (a) NaFSI/MPy shows visible solid and phase separation; (b) NaFSI/MIm is saturated, showing a slight turbidity but is nearly homogeneous; (c) NaFSI/DMIm is fully clear and homogeneous. At right, two complementary simulation snapshots of the NaFSI/MPy system are shown. The smaller box (top) corresponds to an AIMD simulation, capturing the early-stage salt precipitation through pronounced ion clustering, with Na^+ and FSI^- aggregating into salt-rich domains largely excluded from the bulk liquid; consistent with the experimentally observed phase separation. The larger box (bottom) was obtained by CMD, providing a statistically more representative picture of the bulk liquid structure and corroborating the ion segregation and clustering behavior identified by AIMD at a significantly extended length scale.

separation observed experimentally: when MPy fails to stabilize Na^+, the cation remains tightly ion-paired with FSI^-, forming salt-rich aggregates that precipitate from the liquid phase. It is important to note, however, that this RDF is computed from a simulation in which the salt is segregated into a dense domain. As a result, the Na…O signal is inherently biased: it does not reflect the equilibrium coordination in a homogeneous liquid, but rather the local structure within a salt-rich precipitate. The peak intensity and the high Na…O coordination numbers in MPy should therefore be interpreted as structural signatures of salt clustering, not as evidence of a stable solvation environment. The Im system occupies an intermediate position in the Na…O RDF, with a first peak noticeably lower than MPy but higher than DMIm, consistent with its partial but incomplete ability to compete with FSI^- for Na^+ coordination, in agreement with the slight turbidity observed experimentally for NaFSI/Im.

The Na^+ solvation structure in NaFSI/DMIm mixtures was analyzed through AIMD-derived radial distribution functions (RDFs) and coordination numbers (CNs) for the Na…N and Na…O interactions across the three compositions investigated (Fig. 4). Both interactions exhibit a well-defined first coordination peak at approximately 240 pm, consistent with direct Na^+-ligand contact and in agreement with the Na…N distance of ~2.40 Å obtained from static DFT calculations.

Before discussing the structural trends, it is important to address a subtlety inherent to RDF normalization. By definition, the RDF is normalized by the average number density of the reference species in the simulation box, which varies substantially across compositions; the 1:1 system contains significantly more Na^+ per unit volume than the 1:8 system. As a consequence, peak heights in the RDF are sensitive to bulk density and are not directly comparable across compositions as measures of coordination strength or preference. Specifically, a higher RDF peak does not necessarily imply stronger or more frequent coordination; it may simply reflect a denser reference environment. For this reason, the physically meaningful quantity for comparing solvation across compositions is the coordination number CN(r), obtained by integrating the RDF up to its first minimum, as it directly counts the average number of neighbors within the first shell regardless of bulk density effects.

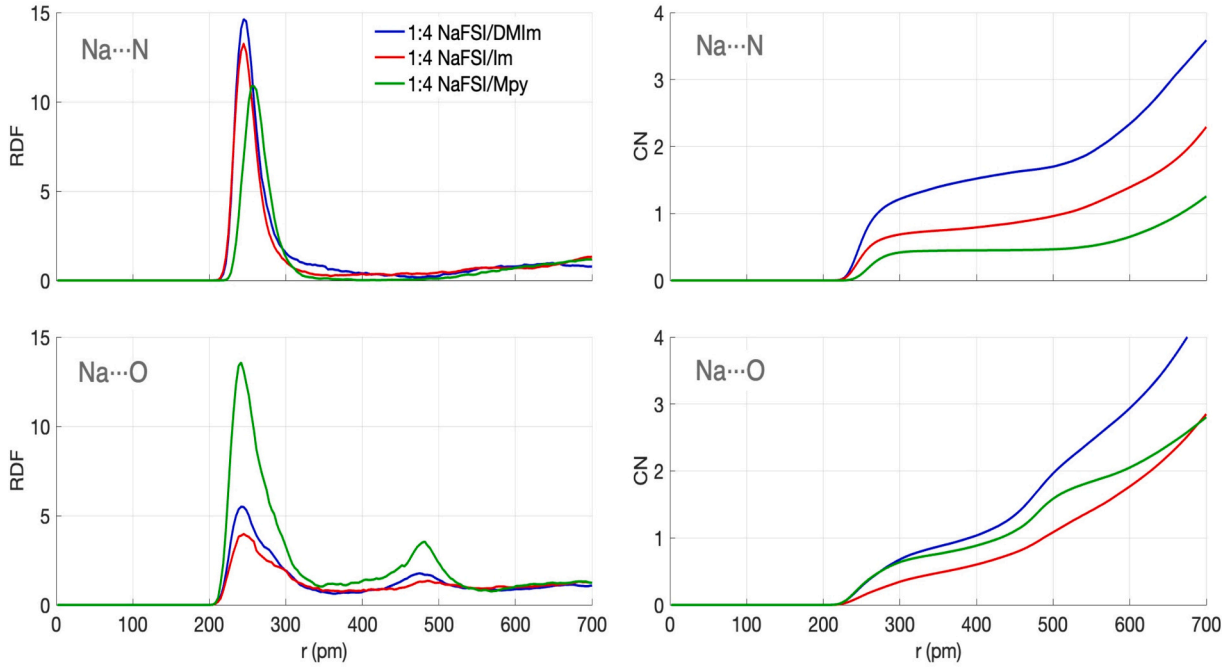

Fig. 3. Radial distribution functions (RDF, left panels) and running coordination numbers (CN, right panels) for Na^+-N (top row) and Na^+-O (bottom row) interactions in the three 1:4 NaFSI:base systems: NaFSI/DMIm (blue), NaFSI/Im (red), and NaFSI/MPy (green), obtained from AIMD simulations. The elevated Na…O signal in MPy should be interpreted as a structural signature of salt clustering within a phase-segregated domain rather than a stable solvation environment. (For interpretation of the references to colour in this figure legend, the reader is referred to the web version of this article.)

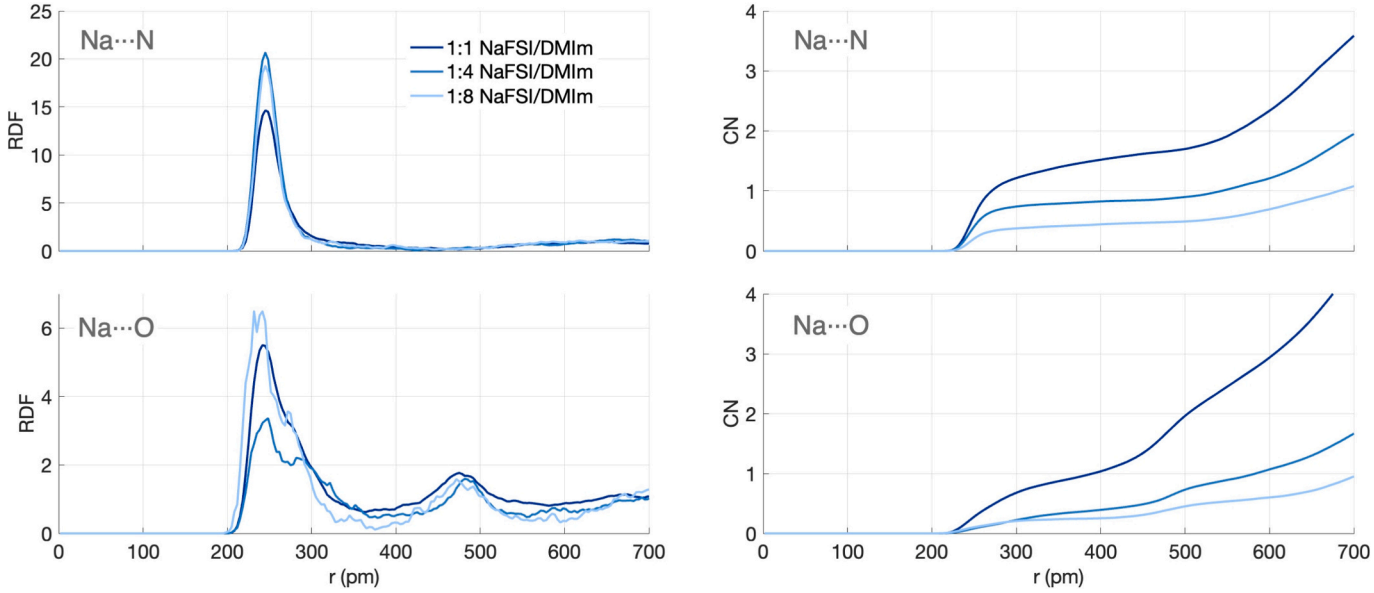

Fig. 4. Radial distribution functions (RDF, left panels) and running coordination numbers (CN, right panels) for Na^+-N (top row) and Na^+-O (bottom row) interactions in NaFSI/DMIm mixtures at three molar ratios (1:1 (dark blue), 1:4 (medium blue), and 1:8 (light blue)) obtained from AIMD simulations. (For interpretation of the references to colour in this figure legend, the reader is referred to the web version of this article.)

With this in mind, the CN trends reveal a clear and consistent picture. For Na…N, the coordination number decreases monotonically with increasing DMIm content: CN(Na…N) = 1.5 (1:1), 0.8 (1:4), and 0.4 (1:8). Similarly, CN(Na…O) decreases from 1.0 (1:1) to 0.4 (1:4) and 0.3 (1:8). Both quantities decrease as DMIm becomes more dilute in Na^+, which is expected: at lower salt concentrations, each Na^+ has fewer neighboring species of any kind within a fixed cutoff distance. The non-monotonic behavior of the RDF peak heights (particularly the maximum of the Na…N peak at 1:4 and the maximum of the Na…O peak at 1:8) is therefore an artifact of the composition-dependent normalization density rather than a physical signature of preferred coordination at intermediate composition.

The key structural insight emerges not from the absolute coordination numbers, but from comparing the observed CNs against those expected for a random, composition-blind distribution of Na^+ neighbors. To this end, Table 2 reports, alongside the observed CN(Na…N) and CN (Na…O), the mole fractions of available coordination sites (x(N), counting only the sp^2 –N=C– nitrogen of each DMIm, and x(O), counting

Table 2
Na^+ coordination numbers in NaFSI/DMIm mixtures at three molar ratios, derived from AIMD simulations. For each composition, the mole fractions of available coordinating sites (x(N), counting the sp^2 –N=C– nitrogen of DMIm, and x(O), counting the four oxygen atoms of FSI^-) are reported alongside the coordination numbers expected under a random site distribution (CN_rand) and the corresponding enrichment factors (CN_obs/CN_rand). Enrichment factors above unity indicate a preference of Na^+ for that coordination site beyond what bulk composition alone would predict.

	1:1	1:4	1:8
x(N)	0.20	0.50	0.67
x(O)	0.80	0.50	0.33
r_{min}(Na…N) (pm)	477	420	453
$CN(Na…N)^{obs}$	1.5	0.8	0.4
$CN(Na…N)^{rand}$	0.50	0.60	0.47
Enrichment N	3.00	1.33	0.86
r_{min}(Na…O) (pm)	380	400	390
$CN(Na…O)^{obs}$	1.0	0.4	0.3
$CN(Na…O)^{rand}$	2.00	0.60	0.23
Enrichment O	0.50	0.67	1.29

the four oxygen atoms of each FSI^-) together with the coordination numbers expected under a random distribution ($CN^{and} = CN_{total} \times x$) and the resulting enrichment factors (CN^{obs} /CN^{rand}). An enrichment factor above unity indicates that Na^+ visits that site more frequently than would be anticipated from the bulk composition alone, reflecting a genuine enthalpic preference.

The results are unambiguous. At the 1:1 composition, nitrogen sites represent only 20% of the available coordinating sites (there are four oxygen atoms for every nitrogen) yet the observed CN(Na…N) = 1.5 is three times larger than the random expectation of 0.50, yielding an enrichment factor of 3.0. This is the strongest evidence in the dataset for an intrinsic Na^+ preference for the sp^2 nitrogen: even when N is the minority species by a factor of four, it dominates the first coordination shell. At 1:4, where N and O sites are equally available, Na^+ still favors nitrogen (enrichment 1.33 vs 0.67 for oxygen), confirming that the preference is not a consequence of DMIm abundance. At 1:8, where nitrogen sites outnumber oxygen sites two-to-one, the enrichment factor for N falls below unity (0.86), while that for O rises slightly above it (1.29). This does not indicate a reversal of preference; rather, it reflects a saturation effect: at high DMIm dilution, the few FSI^- oxygens present are still visited by Na^+ at a rate slightly above the random expectation, suggesting that Na^+-FSI^- electrostatic attraction is never entirely suppressed, but is clearly subordinate to Na…N coordination at all compositions where both sites are meaningfully populated.

Taken together, the enrichment analysis demonstrates that Na^+ exhibits a robust and composition-independent preference for the sp^2 nitrogen of DMIm over FSI^- oxygen. This selective coordination is the molecular event that disrupts Na^+-FSI^- ion pairing, prevents salt clustering, and ultimately drives deep eutectic electrolyte formation.

Considering recent reports that empirical dispersion corrections can alter cation solvation patterns in AIMD, [33] we tested the sensitivity of the Na…N signature to the presence of the Grimme D3 dispersion correction term. Simulations without the D3 contribution show a moderate decrease in the height of the first Na…N peak (~10–15%) without a significant shift in the peak position or a qualitative change in the shape. Integration up to the first minimum indicates that the difference in the coordination number is small (on the order of tenths), within the statistical uncertainty of the trajectories. Consequently, the dispersion correction tends to slightly reinforce the Na…N association, but it does not artificially create the observed coordinated state; the main structural interpretation therefore remains valid. Furthermore, the strong Na…N peak intensities, especially at higher DMIm, imply a preferred binding site on the imidazole ring, whereas the diminishing Na…O peaks show that Na^+-FSI interaction weakens as imidazole becomes available.

The spatial distribution functions (SDFs) shown in Fig. 5 display the three-dimensional probability density of Na^+ around each amine at the 1:4 NaFSI:base composition, computed from AIMD simulations. This present comparison is made at fixed composition across the three ring systems, ensuring that density effects do not confound the interpretation of the isosurfaces. Furthermore, as these SDFs are derived from AIMD trajectories, they inherently capture electronic polarization and charge-transfer effects, lending additional confidence to the directional coordination patterns discussed below.

For DMIm, the Na^+ density is concentrated in a single, well-defined crescent-shaped lobe positioned laterally to the imidazole ring, in close proximity to the –N=C– nitrogen site. This lobe lies within the molecular plane of the ring, directed toward the sp^2 lone pair of the pyridine-like nitrogen. The shape and orientation of this isosurface are characteristic of a directional, localized Na…N coordination interaction: Na^+ approaches the ring from the side of the Lewis-basic nitrogen, following the geometry expected for an ion-dipole interaction with an sp^2 lone pair. A qualitatively identical pattern is observed for imidazole based-system, where the Na^+ density again forms a crescent-shaped lobe oriented toward the imidazole nitrogen, confirming that the coordinating motif is preserved in the absence of *N*-methyl substituents and is an intrinsic property of the aromatic nitrogen site rather than a substituent effect.

Importantly, neither in DMIm nor in Im does the Na^+ density concentrate preferentially above or below the aromatic ring plane; the spatial signature that would be expected if cation-π interactions were the dominant stabilizing motif. The isosurfaces are planar in character, not axial, and do not exhibit the dumbbell-shaped lobes perpendicular to the ring that are typically associated with cation-π geometry. These observations indicate that, while the aromatic character of the imidazole ring is essential for enabling the Lewis-basic sp^2 lone pair at the –N=C– site, the primary Na^+ stabilization mechanism is direct Na…N coordination rather than π-face interaction.

In stark contrast, the MPy system displays a qualitatively different Na^+ distribution. Rather than a single coherent and directional lobe, the isosurface around MPy is fragmented into multiple small, spatially

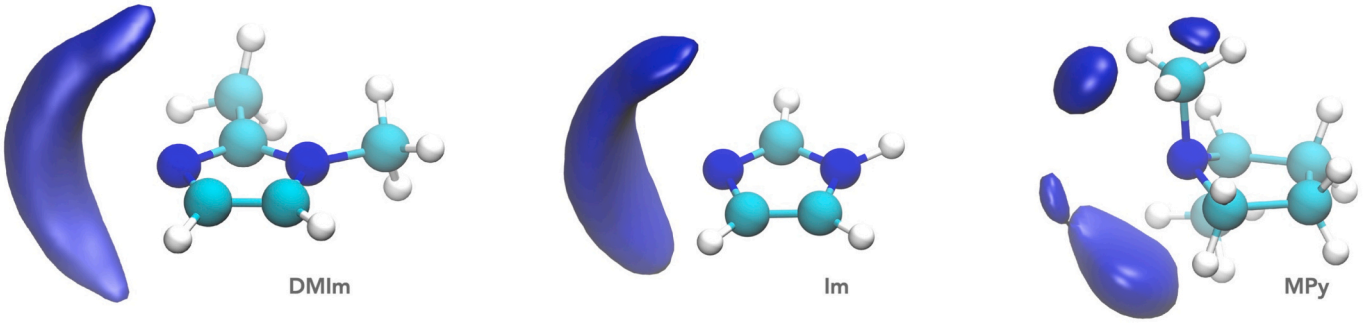

Fig. 5. Spatial distribution functions (SDF) of Na^+ around the three ring systems (DMIm, Im, and MPy) at the 1:4 NaFSI:base composition, derived from AIMD simulations.

disconnected lobes with no clear preferential orientation relative to the nitrogen atom. This diffuse and disordered spatial distribution reflects the absence of a well-defined, electronically accessible coordination site: the sp^3 nitrogen of MPy provides a lone pair embedded in a tetrahedral orbital, which is geometrically less accessible and electronically less polarizing than the sp^2 lone pair of the imidazole derivatives. As a result, Na^+ does not adopt a preferred approach geometry around MPy, and no stable directional coordination is established. This structural incoherence at the molecular level is fully consistent with the macroscopic behavior observed experimentally (NaFSI fails to dissolve in MPy, precipitating as a salt-rich phase) and with the CMD simulations, which show strong ion clustering in the NaFSI/MPy system.

To complement the computational analysis, the macroscopic transport properties of the NaFSI-based deep eutectic electrolytes were measured. In particular, viscosity and ionic conductivity were determined in order to relate the molecular-level insights obtained from AIMD simulations to experimentally accessible transport parameters. The NaFSI/DMIm (1:4) electrolyte exhibits a viscosity of 49.3 ± 3.7 cP and an ionic conductivity of 1.24 ± 0.02 mS·cm^{-1} at 298 K, in good agreement with the values reported by Xiong et al. [6] for the same system (19.6 cP and 1.53 mS·cm^{-1} at ~303 K).

To provide experimental validation beyond the DMIm system, viscosity and ionic conductivity were also measured for NaFSI/MIm (1:4). At 298 K, this mixture exhibits a viscosity of 13.4 ± 2.0 cP and an ionic conductivity of 2.83 ± 0.01 mS·cm^{-1}. The comparatively large uncertainty in the viscosity reflects the presence of a small amount of undissolved solids, consistent with the slight turbidity observed for this system (Fig. 2b) and its proximity to the saturation limit. The lower viscosity and higher conductivity of NaFSI/MIm relative to NaFSI/DMIm can be attributed to the smaller molecular volume and reduced steric hindrance of unsubstituted imidazole. Transport measurements for NaFSI/MPy were not performed, as this system undergoes macroscopic phase separation and does not form a single liquid phase (Fig. 2a). Taken together, these results demonstrate that both aromatic imidazole-based systems form functional electrolytes with competitive ionic transport, while the non-aromatic amine fails to produce a liquid amenable to characterization.

The transport data were used to prepare a Walden plot where the ionicity of the NaFSI/DMIm DEE is compared with other DES previously reported in the literature by Wang et al. [34], as shown in Fig. 6.

The Walden plot provides a framework to compare ion transport in complex liquids by relating molar conductivity to fluidity. When the NaFSI-based systems are compared to a wide range of DES, a clear trend appears. The NaFSI systems (highlighted as blue + markers on a yellow background) are located above most of the DES data points and lie closer to the ideal Walden line, which represents fully dissociated electrolytes with optimal ionic mobility. In addition, they are positioned toward the right-hand side of the plot, corresponding to high fluidities (i.e., low viscosities). This placement in the Walden plot indicates that, for a given viscosity, the NaFSI systems exhibit higher molar conductivity than conventional DES, and a higher ionicity. This means that a larger fraction of the species present in the liquid are free, mobile charge carriers contributing effectively to electrical conduction. This behavior stands in contrast to most DES, which are “poor ionic” systems due to strong intermolecular interactions and limited availability of free ions.

The origin of this enhanced ionicity in NaFSI systems can be traced to their molecular interactions discussed above in this work. Unlike classical DES, which are dominated by extensive hydrogen-bond networks and the formation of neutral or weakly charged aggregates, NaFSI-based systems are governed primarily by metal-ligand coordination, specifically Na…N interactions with the imidazole. These interactions are sufficiently strong to structure the liquid but remain more labile than the persistent hydrogen-bond networks found in DES. As a result, long-lived ion pairing is reduced, and the system avoids the formation of tightly bound aggregates that would otherwise hinder ion mobility. This leads to a situation where ions are more weakly associated and can move more easily through the liquid. Consequently, the NaFSI systems behave much more like true electrolytes, where charge transport is dominated by quasi-free ions rather than correlated or clustered species.

A comparison with lithium-based systems further highlights this

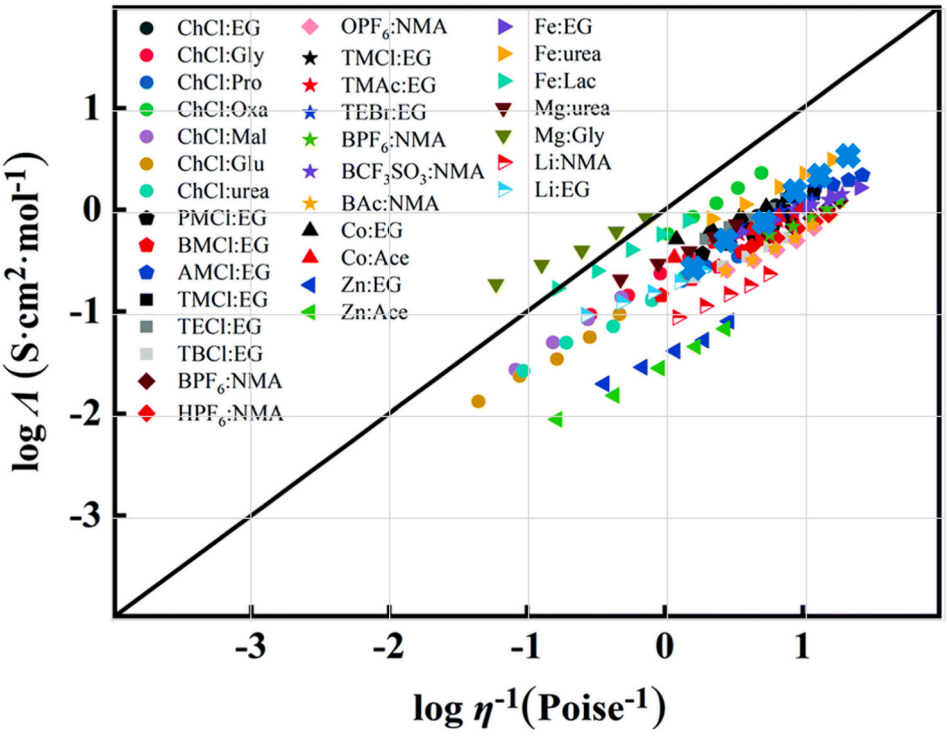

Fig. 6. Walden plot for NaFSI/DMIm DEEs (blue + on yellow background) and its comparison with other DES from reference [38]. (For interpretation of the references to colour in this figure legend, the reader is referred to the web version of this article.)

distinction. In the Walden plot, Li-based DES (such as LiTFSI:NMA or LiTFSI:EG) are located below the NaFSI systems. This shows both lower ionicity and reduced transport efficiency. The reduced performance of Li systems is attributed to stronger ion pairing and solvation effects, as well as the large size of the TFSI anion. Wang et al. [34] reported that LiTFSI:NMA displays low ionicity specifically due to the bulky $TFSI^-$ anion, which promotes ion association and limits the number of free charge carriers. As a result, lithium-based systems seem to be less efficient in conducting charge under comparable conditions.

Taken together, these observations demonstrate that NaFSI systems behave fundamentally differently from both conventional DES and lithium-based analogues. They are less dominated by hydrogen-bonded aggregation and more closely resemble concentrated electrolytes in their transport characteristics. Most importantly, they exhibit significantly higher effective conductivity than both DES and Li-based systems, owing to their higher ionicity and greater number of mobile charge carriers. This enhanced ion transport is expected to translate into improved rate capability and reduced polarization in sodium-ion batteries, highlighting the potential of these coordination-driven electrolytes for high-performance energy storage applications.

4. Conclusions

This work establishes that the sp^2 hybridization of the coordinating nitrogen, enabled by ring aromaticity, is the decisive molecular feature behind NaFSI solvation and deep eutectic electrolyte formation. Experimentally, NaFSI dissolves readily in aromatic imidazole derivatives (DMIm, Im) but phase-separates in the non-aromatic amine MPy, demonstrating a direct link between amine electronic structure and macroscopic miscibility.

AIMD simulations provide a molecular-level explanation. In DMIm and Im, Na^+ forms a well-defined, directional coordination with the sp^2 lone pair of the –N=C– nitrogen, evidenced by sharp Na…N RDF peaks and spatially coherent Na^+ probability distributions. In MPy, the sp^3 nitrogen fails to establish directed coordination, leaving Na^+ predominantly ion-paired with FSI^-; a structural signature of salt clustering consistent with the observed phase separation. Across NaFSI/DMIm compositions, coordination numbers reveal a monotonic exchange of Na…O contacts for Na…N contacts as DMIm increases, confirming a genuine enthalpic preference for imidazole nitrogen coordination that progressively displaces FSI^- from the first solvation shell and stabilizes the liquid phase.

The resulting NaFSI/DMIm electrolyte exhibits moderate viscosity and measurable ionic conductivity at ambient temperature, with enhanced ionicity compared to conventional deep eutectic solvents. These transport properties are consistent with a coordination-driven liquid structure that promotes mobile charge carriers, which is desirable for sodium-ion battery operation. Moreover, the 3.2 V electrochemical stability window previously reported for this system [6] is consistent with the strong, directional Na…N coordination identified here, which displaces FSI^- from the first solvation shell and is expected to delay anion decomposition at the electrode interface.

These findings, drawn from a controlled comparison that isolates aromaticity and nitrogen hybridization as the single structural variable (aromatic DMIm and Im vs. non-aromatic MPy), point to a clear molecular design principle for sodium-based deep eutectic electrolytes: effective solvation of Na^+ requires a coordinating nitrogen with sp^2 character within an aromatic framework. While the present study is based on three representative systems, the underlying mechanism (directional Lewis-base coordination through an accessible sp^2 lone pair) is a transferable electronic-structure feature rather than a system-specific effect, and its generality should be tested across a broader family of aromatic nitrogen donors such as pyridine, pyrazole, and triazole derivatives.

CRediT authorship contribution statement

Eudes Eterno Fileti: Methodology, Investigation, Formal analysis, Data curation, Conceptualization. **Luis G. Dias:** Investigation, Conceptualization. **G. Camilo:** Investigation, Formal analysis, Conceptualization. **Dinis O. Abranches:** Methodology, Investigation, Formal analysis, Conceptualization. **João A.P. Coutinho:** Supervision, Resources, Project administration, Methodology, Investigation, Funding acquisition, Formal analysis, Conceptualization.

Declaration of Generative AI and AI-assisted technologies in the writing process

The authors used a generative AI tool solely to improve the clarity and language of the manuscript. The AI tool was not used to generate scientific content, interpret data, or draw conclusions. The authors take full responsibility for the content of the manuscript.

Declaration of competing interest

The authors declare that they have no known competing financial interests or personal relationships that could have appeared to influence the work reported in this paper. The funding sources had no involvement in the study design; in the collection, analysis and interpretation of data; in the writing of the report; or in the decision to submit the article for publication.

Acknowledgments

This work was developed within the scope of the project CICECO-Aveiro Institute of Materials, UID/50011/2025 (DOI 10.54499/UID/50011/2025) & LA/P/0006/2020 (DOI 10.54499/LA/P/0006/2020), financed by national funds through the FCT/MCTES (PIDDAC). E.E.F thanks Brazilian agencies FAPESP and CNPq for support. JAPC and EEF acknowledge FCT for the financial support through Grant Agreement nº FCT/Mobility/1335482321/2024-25. This work was partially supported by the Laboratório Nacional de Computação Científica (LNCC, Brazil), providing HPC resources of the Santos Dumont supercomputer.

Data availability

No data was used for the research described in the article.

References

[1] J.-Y. Hwang, S.-T. Myung, Y.-K. Sun, Sodium-ion batteries: present and future, Chem. Soc. Rev. 46 (2017) 3529–3614, https://doi.org/10.1039/C6CS00776G.
[2] H. Pan, Y.-S. Hu, L. Chen, Room-temperature stationary sodium-ion batteries for large-scale electric energy storage, Energy Environ. Sci. 6 (2013) 2338, https://doi.org/10.1039/c3ee40847g.
[3] W. Chen, T. Lei, C. Wu, M. Deng, C. Gong, K. Hu, Y. Ma, L. Dai, W. Lv, W. He, X. Liu, J. Xiong, C. Yan, Designing safe electrolyte systems for a high-stability lithium–sulfur battery, Adv. Energy Mater. 8 (2018), https://doi.org/10.1002/aenm.201702348.
[4] D.O. Abranches, J.A.P. Coutinho, Everything you wanted to know about deep eutectic solvents but were afraid to be told, Annu. Rev. Chem. Biomol. Eng. 14 (2023) 141–163, https://doi.org/10.1146/annurev-chembioeng-101121-085323.
[5] D. Monti, E. Jónsson, M.R. Palacín, P. Johansson, Ionic liquid based electrolytes for sodium-ion batteries: Na+ solvation and ionic conductivity, J. Power Sources 245 (2014) 630–636, https://doi.org/10.1016/j.jpowsour.2013.06.153.
[6] W. Xiong, X. Zhang, Z. Tu, X. Hu, Y. Wu, Novel deep eutectic electrolyte induced by Na···N interactions for sodium batteries, Ind. Eng. Chem. Res. 62 (2023) 51–61, https://doi.org/10.1021/acs.iecr.2c03313.
[7] A.-S. Kelchtermans, D. De Sloovere, J. Mercken, T. Vranken, G. Mangione, B. Joos, W. Vercruysse, D. Vandamme, H. Hamed, M. Safari, E. Derveaux, P. Adriaensens, M.K. Van Bael, A. Hardy, Superconcentration strategy allows sodium metal compatibility in deep eutectic solvents for sodium-ion batteries, ACS Omega 9 (2024) 42343–42352, https://doi.org/10.1021/acsomega.4c02896.
[8] D. Chen, Y. Wang, T. Yao, H. Yang, L. Shen, Unraveling the exceptional kinetics of Zn||organic batteries in hydrated deep eutectic solution, J. Energy Chem. 101 (2025) 570–577, https://doi.org/10.1016/j.jechem.2024.10.016.

[9] L. Wang, Y. Deng, L. Yan, Low-cost "water-in-deep eutectic solvent" electrolyte for high-performance zinc ion hybrid supercapacitors, ACS Appl. Energy Mater. 6 (2023) 10585–10592, https://doi.org/10.1021/acsaem.3c01737.
[10] F. D'Anna, P. Vitale, R. Noto, Determination of basic strength of aliphatic amines through ion pair formation in some ionic liquid solutions, J. Organomet. Chem. 74 (2009) 6224–6230, https://doi.org/10.1021/jo901172j.
[11] Y. Huang, G. Qiu, Z. Tai, Y. Liu, Deep eutectic solvent-based gel electrolyte with fast Na ions transport in sodium-metal batteries, ChemSusChem 18 (2025), https://doi.org/10.1002/cssc.202500417.
[12] D. Marx, J. Hutter, Ab initio molecular dynamics, Cambridge University Press, 2009, https://doi.org/10.1017/CBO9780511609633.
[13] M. Shakourian-Fard, H.R. Ghenaatian, S. Pasban, G. Kamath, *In silico* navigation of Na^+ ion solvation in deep eutectic solvents to propel the next wave of sodium-ion battery electrolytes, J. Mater. Chem. A Mater. 13 (2025) 33442–33456, https://doi.org/10.1039/D5TA03220B.
[14] F. Philippi, D. Rauber, K.L. Eliasen, N. Bouscharain, K. Niss, C.W.M. Kay, T. Welton, Pressing matter: why are ionic liquids so viscous? Chem. Sci. 13 (2022) 2735–2743, https://doi.org/10.1039/D1SC06857A.
[15] F. Lundin, A. Idström, P. Falus, L. Evenäs, S. Xiong, A. Matic, Ion dynamics and nanostructures of diluted ionic liquid electrolytes, J. Phys. Chem. C 126 (2022) 16262–16271, https://doi.org/10.1021/acs.jpcc.2c04503.
[16] L. Martínez, R. Andrade, E.G. Birgin, J.M. Martínez, P <scp>ACKMOL</scp> : a package for building initial configurations for molecular dynamics simulations, J. Comput. Chem. 30 (2009) 2157–2164, https://doi.org/10.1002/jcc.21224.
[17] W.L. Jorgensen, D.S. Maxwell, J. Tirado-Rives, Development and testing of the OPLS all-atom force field on conformational energetics and properties of organic liquids, J. Am. Chem. Soc. 118 (1996) 11225–11236, https://doi.org/10.1021/ja9621760.
[18] M.J. Abraham, T. Murtola, R. Schulz, S. Páll, J.C. Smith, B. Hess, E. Lindahl, GROMACS: high performance molecular simulations through multi-level parallelism from laptops to supercomputers, SoftwareX 1–2 (2015) 19–25, https://doi.org/10.1016/j.softx.2015.06.001.
[19] A.D. Becke, Density-functional exchange-energy approximation with correct asymptotic behavior, Phys. Rev. A 38 (1988) 3098–3100, https://doi.org/10.1103/PhysRevA.38.3098.
[20] C. Lee, W. Yang, R.G. Parr, Development of the Colle-Salvetti correlation-energy formula into a functional of the electron density, Phys. Rev. B 37 (1988) 785–789, https://doi.org/10.1103/PhysRevB.37.785.
[21] S. Grimme, J. Antony, S. Ehrlich, H. Krieg, A consistent and accurate *ab initio* parametrization of density functional dispersion correction (DFT-D) for the 94 elements H-Pu, J. Chem. Phys. 132 (2010), https://doi.org/10.1063/1.3382344.
[22] M. Brehm, M. Thomas, Computing bulk phase Raman optical activity spectra from *ab initio* molecular dynamics simulations, J. Phys. Chem. Lett. 8 (2017) 3409–3414, https://doi.org/10.1021/acs.jpclett.7b01616.
[23] D.A.C. da Silva, G. Colherinhas, E.E. Fileti, Atomic-scale insights into phosphorene-ionic liquid Interface with ab initio molecular dynamics, ACS Phys. Chem. Au 6 (2026) 207–214, https://doi.org/10.1021/acsphyschemau.5c00111.
[24] E.E. Fileti, H. de A. Chagas, G. Colherinhas, T. Malaspina, Quantum molecular dynamics approach to understanding interactions in betaine chloride and amino acid natural deep eutectic solvents, ACS Phys. Chem. Au 5 (2025) 72–79, https://doi.org/10.1021/acsphyschemau.4c00072.
[25] E. Eterno Fileti, I.V. Voroshylova, E.S.C. Ferreira, M. Natália D.S. Cordeiro, T. Malaspina, Ab initio molecular dynamics study of hydroxyl positioning in butanediol and its impact on deep eutectic solvent structure, J. Mol. Liq. 409 (2024) 125548, https://doi.org/10.1016/j.molliq.2024.125548.
[26] S. Goedecker, M. Teter, J. Hutter, Separable dual-space Gaussian pseudopotentials, Phys. Rev. B 54 (1996) 1703–1710, https://doi.org/10.1103/PhysRevB.54.1703.
[27] J. VandeVondele, J. Hutter, Gaussian basis sets for accurate calculations on molecular systems in gas and condensed phases, J. Chem. Phys. 127 (2007), https://doi.org/10.1063/1.2770708.
[28] T.D. Kühne, M. Iannuzzi, M. Del Ben, V.V. Rybkin, P. Seewald, F. Stein, T. Laino, R. Z. Khaliullin, O. Schütt, F. Schiffmann, D. Golze, J. Wilhelm, S. Chulkov, M. H. Bani-Hashemian, V. Weber, U. Borštnik, M. Taillefumier, A.S. Jakobovits, A. Lazzaro, H. Pabst, T. Müller, R. Schade, M. Guidon, S. Andermatt, N. Holmberg, G.K. Schenter, A. Hehn, A. Bussy, F. Belleflamme, G. Tabacchi, A. Glöß, M. Lass, I. Bethune, C.J. Mundy, C. Plessl, M. Watkins, J. VandeVondele, M. Krack, J. Hutter, CP2K: an electronic structure and molecular dynamics software package - Quickstep: efficient and accurate electronic structure calculations, J. Chem. Phys. 152 (2020), https://doi.org/10.1063/5.0007045.
[29] M. Brehm, B. Kirchner, TRAVIS-A free analyzer and visualizer for Monte Carlo and Molecular dynamics trajectories, J. Chem. Inf. Model. 51 (2011) 2007–2023, https://doi.org/10.1021/ci200217w.
[30] D.A. Shultz, A.K. Boal, N.P. Campbell, Effect of aliphatic amine bases on the aggregation of alkali metal salts of 3,5-Di- *tert* -butylsemiquinone (3,5-DBSQ), Inorg. Chem. 37 (1998) 1540–1543, https://doi.org/10.1021/ic971113v.
[31] Y. Hirotsu, M.L. Thomas, Y. Takeoka, M. Rikukawa, M. Yoshizawa-Fujita, Effect of cation side-chain structure on the physicochemical properties of pyrrolidinium-based electrolytes upon mixing with sodium salt, Sci. Technol. Adv. Mater. 26 (2025), https://doi.org/10.1080/14686996.2025.2466417.
[32] D.T. Infield, A. Rasouli, G.D. Galles, C. Chipot, E. Tajkhorshid, C.A. Ahern, Cation-π interactions and their functional roles in membrane proteins, J. Mol. Biol. 433 (2021) 167035, https://doi.org/10.1016/j.jmb.2021.167035.
[33] V. Kostal, P.E. Mason, H. Martinez-Seara, P. Jungwirth, Common cations are not polarizable: effects of dispersion correction on hydration structures from ab initio molecular dynamics, J. Phys. Chem. Lett. 14 (2023) 4403–4408, https://doi.org/10.1021/acs.jpclett.3c00856.
[34] Y. Wang, W. Chen, Q. Zhao, G. Jin, Z. Xue, Y. Wang, T. Mu, Ionicity of deep eutectic solvents by Walden plot and pulsed field gradient nuclear magnetic resonance (PFG-NMR), Phys. Chem. Chem. Phys. 22 (2020) 25760–25768, https://doi.org/10.1039/D0CP01431A.